

Double-Weyl Phonons in Transition-Metal Monosilicides


Tiantian Zhang,^{1,4} Zhida Song,^{1,4} A. Alexandradinata,² Hongming Weng,^{1,3} Chen Fang,^{1,*} Ling Lu,^{1,†} and Zhong Fang^{1,3}

¹*Institute of Physics, Chinese Academy of Sciences/Beijing National Laboratory for Condensed Matter Physics, Beijing 100190, China*

²*Department of Physics, Yale University, New Haven, Connecticut 06520, USA*

³*Collaborative Innovation Center of Quantum Matter, Beijing 100084, China*

⁴*University of Chinese Academy of Sciences, Beijing 100049, China*

 (Received 25 June 2017; published 5 January 2018)

We employed *ab initio* calculations to identify a class of crystalline materials of MSi ($M = \text{Fe, Co, Mn, Re, Ru}$) having double-Weyl points in both their acoustic and optical phonon spectra. They exhibit novel topological points termed “spin-1 Weyl point” at the Brillouin zone center and “charge-2 Dirac point” at the zone corner. The corresponding gapless surface phonon dispersions are two helicoidal sheets whose isofrequency contours form a single noncontractible loop in the surface Brillouin zone. In addition, the global structure of the surface bands can be analytically expressed as double-periodic Weierstrass elliptic functions.

DOI: [10.1103/PhysRevLett.120.016401](https://doi.org/10.1103/PhysRevLett.120.016401)

Topological states of electrons [1–4] and photons [5,6] have attracted significant interest recently. Topological mechanical states [7–21], also being actively explored, have only been limited to low-energy classical sound waves at kHz frequencies in macroscopic artificial lattices. However, the important processes like heat conduction and electron-phonon coupling are all determined by THz phonons of atomic lattice vibrations, whose force constants have to be evaluated quantum mechanically. In this Letter, we explore crystalline materials in the noncentrosymmetric space group $P2_13$ (No.198), whose threefold representation at Brillouin zone (BZ) center and fourfold representations at BZ edge are point degeneracies of Chern number 2. A class of transition-metal monosilicides are consequently found to host such double Weyl points throughout their phonon spectrum of terahertz frequencies. The double-Weyl surface states are explicitly calculated and can be analytically described by the Weierstrass elliptic function. Our prediction of topological bulk and surface phonons can be experimentally verified by many techniques [22] such as neutron scattering [23] for bulk phonons and electron energy loss spectroscopy [24] for surface phonons. This work paves the way for topological phononics [25–28] at the atomic scale.

Double Weyl points.— The two-band Hamiltonian near a Weyl point [29–36] [Fig. 1(a)], $H_2(\mathbf{k}) \propto \mathbf{k} \cdot \mathbf{S} = (\hbar/2)\mathbf{k} \cdot \boldsymbol{\sigma}$, is the simplest possible Lorentz invariant theory for three-dimensional (3D) massless fermions, where \mathbf{S} is the rotation generator for spin-1/2 particles and σ_i 's are the Pauli matrices. The two bands have spin components $S_k = \mathbf{S} \cdot \hat{\mathbf{k}} = +\hbar/2$ and $-\hbar/2$ and form inward or outward hedgehog configuration on each equal-energy surface. The Chern number of +1 or –1 is the topological invariant that distinguishes between these two cases. For spin-1 bosons like phonon, photon and magnons, the natural

extension of a Weyl Hamiltonian is the three-band Hamiltonian $H_3(\mathbf{k}) \propto \mathbf{k} \cdot \mathbf{L}$ [Fig. 1(c)], where L_i are the spin-1 matrix representations of the rotation generators. The Chern numbers of the resultant three bands, corresponding to $L_k = \mathbf{L} \cdot \hat{\mathbf{k}} = \hbar, 0, -\hbar$ are +2, 0 and –2, doubling those of the spin-1/2 Weyl point. We hence refer to such a band crossing point as the “spin-1 Weyl point” [37] in this paper. Another possibility of band crossing having Chern number of 2 is the direct sum of two identical spin-1/2 Weyl points, referred to as “charge-2 Dirac point” in this paper [Fig. 1(d)], whose four-band Hamiltonian is $H_4(k) \sim \begin{pmatrix} k \cdot \boldsymbol{\sigma} & 0 \\ 0 & k \cdot \boldsymbol{\sigma} \end{pmatrix}$ [38], in contrast to a regular 3D Dirac point consists of two Weyl points of opposite Chern numbers [39] and quadratic double-Weyl points between two bands [40–43] [Fig. 1(b)]. In the following, we show the presence of the spin-1 Weyl and charge-2 Dirac points in the phonon spectra of existing materials.

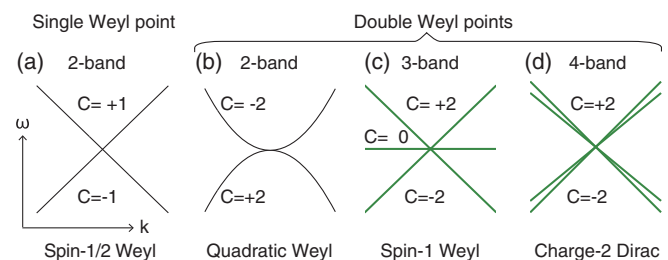


FIG. 1. Single Weyl point and two types of double-Weyl points. (a) A spin-1/2 Weyl point of Chern number of ± 1 . (b) The 2-band quadratic Weyl point with Chern numbers of ± 2 . (c) The 3-band spin-1 Weyl point with Chern numbers of 0, ± 2 . (d) The 4-band charge-2 Dirac point with Chern numbers ± 2 . Here we refer to quadratic Weyl point, spin-1 Weyl point and charge-2 Dirac points as double Weyl points. We focus on the 3-band and 4-band double Weyl points in this paper.

Phonon calculations.— Phonons are quantized excited vibrational states of interacting atoms. Solids with more than one atom in the primitive cell have both acoustic and optical branches in their phonon band structure, which we computed for the MSi family ($M = Fe, Co, Mn, Re, Ru$) in Fig. 2. MSi belongs to the simple cubic crystal structure with space group $P2_13$ (No. 198). Each primitive cell contains 8 atoms, both M and Si atoms occupy Wyckoff positions (4a). The crystal structure of MSi [44,45] is shown in Fig. 2(a) and the corresponding BZ is shown in Fig. 2(b). In this paper, the phonon force constants are calculated based on density functional perturbation theory [46], using Vienna *ab initio* simulation package (VASP) [47]. Wilson loop method [48,49] is used to find the Chern numbers of the double-Weyl points.

Spin-1 Weyl acoustic phonons.— Shown in Fig. 2(c), the three branches of acoustic phonons form a spin-1 Weyl

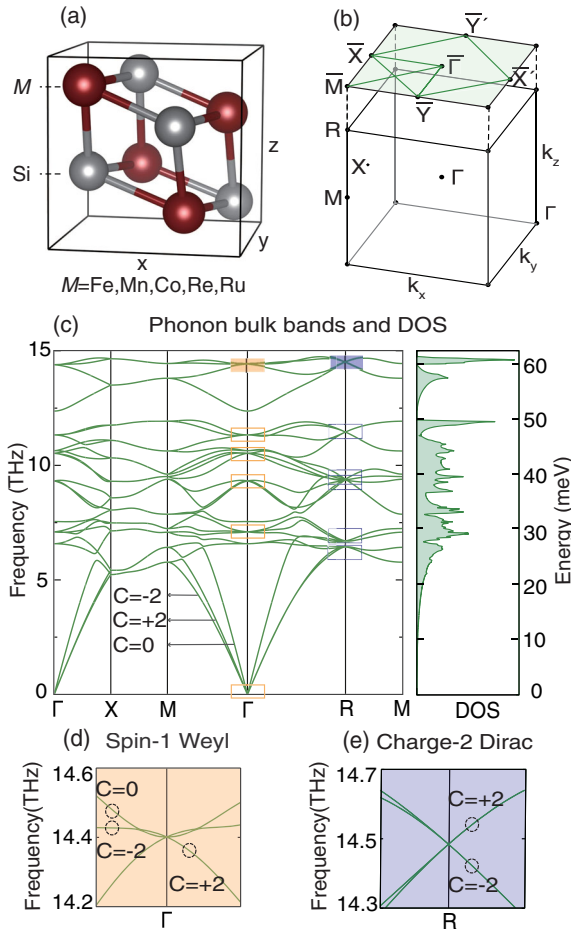


FIG. 2. MSi crystal structure and phonon bands. (a) Cubic unit cell contains 4 M and 4 Si atoms. (b) Bulk and (001) surface BZs. (c) Phonon dispersion of $FeSi$ along high-symmetry directions. The acoustic bands have Chern numbers of $0, \pm 2$. The orange boxes are centered around the spin-1 Weyl points at Γ and the purple boxes are centered around the charge-2 Dirac points at R . (d) Γ point is a spin-1 Weyl point. (e) R point is a charge-2 Dirac point.

point. The longitudinal branch has a Chern number of 0 and the two transverse branches have Chern numbers of ± 2 , reflecting the fact that phonons are spin-1 particles. We note that the individual Chern numbers can be defined only when the three acoustic dispersions are well separated from each other. This only happens when \mathcal{PT} symmetry is broken, since, otherwise, Berry curvature strictly vanishes and the Chern number of any band is zero. Here \mathcal{P} is parity inversion and \mathcal{T} is time reversal. MSi is noncentrosymmetric, so \mathcal{P} is broken in the lattice. We emphasize that these spin-1 Weyl dispersions is a general property for both phonons and photons at zero frequency; the difference lies in the vanishing longitudinal mode for photons [50]. We note that the topological surface states related to this zero-frequency spin-1 Weyl point may not be observed, since the two transverse Chern bands both have positive group velocity in all directions, not leaving a bulk gap when projected on any open surface.

Double-Weyl optical phonons.— Both the spin-1 Weyl points at Γ and charge-2 Dirac points at R were found in the optical phonon spectrum of $FeSi$ in Fig. 2(c). They are stabilized by the lattice symmetries and \mathcal{T} . The No. 198 ($P2_13$) space group has twofold screw rotations along each $\langle 100 \rangle$ axes ($\{C_{2x} | (\frac{1}{2}, \frac{1}{2}, 0)\}$ along x axis) and threefold rotations C_3 along the $\langle 111 \rangle$ axes. We performed a $k \cdot p$ analysis at the two \mathcal{T} -invariant momenta of Γ and R (see Sec. IV of the Supplemental Material [51] for details).

At the Γ point, the irreducible representations for the optical branches are $\Gamma = 2A + 2E + 5T$, in which A , E , and T represent the singly, doubly, and triply degenerate multiplets, respectively. All five threefold band degeneracies are spin-1 Weyl points enforced by the little group symmetry at Γ , which is the point group $T(23)$. The polariton effect of LO-TO splitting is discussed in the Supplemental Material [51].

At the R point of the BZ corner, all bands form charge-2 Dirac points. In other words, in MSi materials, every phonon band connects to the fourfold degenerate double-Weyl points at R . This is due to both \mathcal{T} and the non-symmorphic nature of the No. 198 space group containing three screw axes.

As examples, we plotted the closeup dispersions of the two types of double-Weyl points of the highest phonon bands (~ 14.5 THz) in Figs. 2(d) and 2(e). These four bands are frequency isolated from the rest. Since a topological point carrying nonzero Chern number cannot exist alone in the BZ, the spin-1 Weyl and charge-2 Dirac points come in pairs and their Chern numbers cancel exactly.

Here we offer an intuitive perspective to understand the charge-2 Dirac point at R . The three screw axes, $C_{2x,2y,2z}$, at this point anticommute with each other and satisfy $C_{2i}^2 = -1$, just like half-integer spin rotations. From this we know that all irreducible representations have even dimensions, with the smallest representation being two dimensional and the rotations represented by $\pm i\sigma_{x,y,z}$.

But since R is also time-reversal invariant, these screw axes must commute with \mathcal{T} , so that all matrix representations of the three screws must be real. This is impossible for two-dimensional representations of $SU(2)$, but can be met by four-dimensional representations. Finally, since time reversal preserves the Chern number of a Weyl point, the four-dimensional representation has charge ± 2 .

Single noncontractible surface loop.— An isoenergy contour of any 2D (noninteracting) system or trivial surface state is a closed loop, which can be continuously deformed into an even number of noncontractible loops which wraps around the BZ torus. The unique feature of a Weyl crystal is its open surface arcs whose ends are pinned by the projection of Weyl points in the bulk. In contrast, the MSi surface contour is a single noncontractible loop.

The surface local density of states (LDOS) is plotted along the surface momentum lines in Fig. 3(a) and the iso-frequency surface contours are plotted in Figs. 3(b), 3(c), and 3(d) for different frequencies. For computing the surface LDOS, we first calculated the second rank tensor of force constant in Cartesian coordinates from density functional perturbation theory, from which we can get the tight-binding parameters for the bulk and surface atoms. [52]. Then we obtain the surface Green's function iteratively and take its imaginary part as the LDOS [53–55].

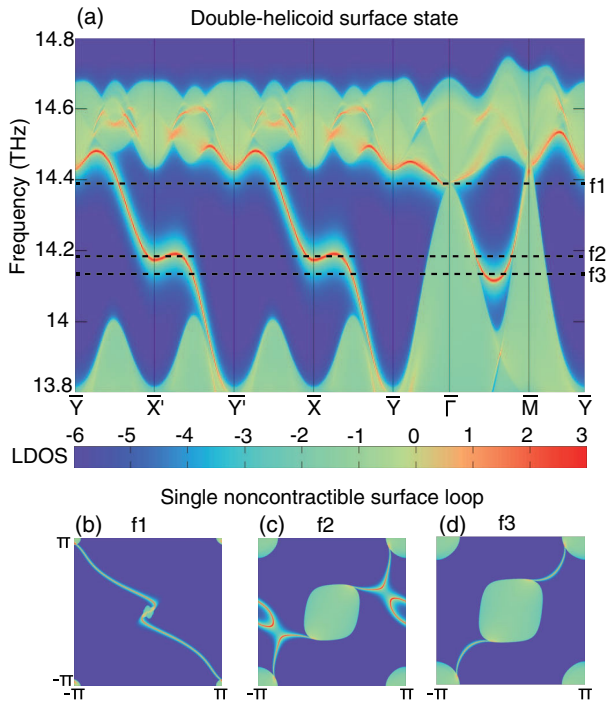


FIG. 3. Double-helicoid surface states and noncontractible surface arcs. (a) The surface LDOS for the (001) surface along high-symmetry directions. The corresponding surface arcs for different frequency are showed in (b)–(d), plotted in the log scale. There are two arcs rotates around the two double Weyl points as the frequency decreases from f_1 to f_3 , which demonstrates the double-helical surface states.

On the (001) surface, the symmetries of the MSi lattice are broken on the surface and \mathcal{T} is the only symmetry left invariant other than the in-plane translations. The (001) surface BZ is a square. The spin-1 Weyl point at Γ is projected to $\bar{\Gamma}$, and the charge-2 Dirac point at R is projected to \bar{M} . Note that the four BZ corners are the same \bar{M} point. Since surface arcs always connect two Weyl points with opposite Chern numbers, there should be two arcs connecting the double-Weyl points at the BZ center ($\bar{\Gamma}$) and BZ corner (\bar{M}). Constrained by \mathcal{T} , the two arcs must be related by a π rotation about Γ ; when viewed together, the two arcs stretch diagonally across the BZ. This forms a single noncontractible loop connected by two surface arcs where the connection points are projections of the bulk double-Weyl points. These novel noncontractible surface loops are shown at three different frequencies in Figs. 3(b), 3(c), and 3(d), where the bulk pockets are connected by the two arcs.

Double-helicoid surface states.— Isoenergy surface arcs are only the local description (in energy) of a topological surface state in the momentum space, which are gapless under arbitrary surface conditions, in the presence of the protecting symmetries. They are sheets noncompact (not bounded) and gapless along the frequency axis. Fang *et al.* [56] pointed out that the Weyl surface states are equivalent to a helicoid, one of the common noncompact Riemann sheets. Here, it is natural to expect that the surface state of a double-Weyl crystal is a double helicoid: two surface sheets wind around the double Weyl point. This is indeed confirmed by the results plotted in Fig. 3 and illustrated in Fig. 4.

Analytical description by Weierstrass elliptic function.— We show that the double-helicoid surface of MSi phonons

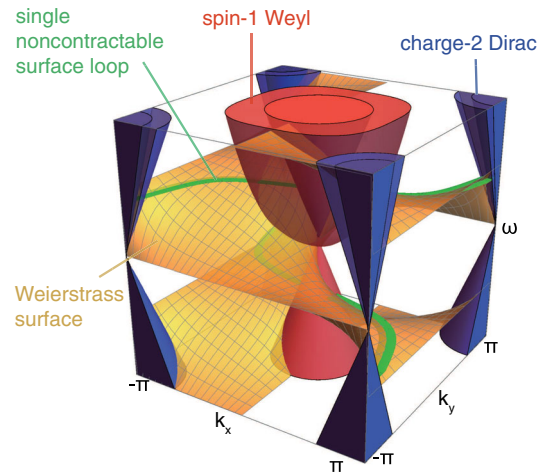


FIG. 4. The double-helicoid surface state is described by the Weierstrass elliptic function. The red spin-1 Weyl point corresponds to the double zero point and the blue charge-2 Dirac point corresponds to the double pole point. Two yellow surfaces rotate around these two double-Weyl points as double helicoids.

is topologically equivalent to the Weierstrass elliptic function, that is double-periodic and analytical in the whole BZ. In Ref. [56], Fang *et al.* showed that the surface state dispersion near the projection of topological band crossings can be mapped to the Riemann surfaces of analytic functions with surface momentum $k \equiv k_x + ik_y$ as a complex variable. Near the projection of a Weyl point having Chern number (C), the dispersion is topologically equivalent to the winding phase of an analytic function having an order- C zero ($C > 0$) or pole ($C < 0$), or symbolically $\omega(z) \sim \text{Im}[\log(z^C)]$, where z is the planar momentum relative to the projection of the Weyl point.

However, this analytic functions z^C is defined in a noncompact momentum space and hence cannot provide a global description for surface dispersions in the whole surface BZ, which is a compact torus. To establish the global picture, we notice that analytic functions having two or more zero-pole pairs and are periodic in both directions are elliptic functions. Therefore, we use the Weierstrass elliptic function (\wp), having one second-order pole at $\mathbf{k}_+ = (\pi, \pi)$ and one second-order zero at $\mathbf{k}_- = (0, 0)$, to reveal the global structure of the double-Weyl surface states. The explicit mapping is given by

$$\begin{aligned} \omega(k_x, k_y) &\sim \wp(z; 2\pi, 2\pi) \\ &= \text{Im} \left\{ \log \left[\frac{1}{z^2} + \sum_{n,m \neq 0} \left(\frac{1}{(z + 2m\pi + 2n\pi i)^2} - \frac{1}{(2m\pi + 2n\pi i)^2} \right) \right] \right\}, \end{aligned} \quad (1)$$

where $z \equiv k - (1 + i)\pi$.

We plot, in Fig. 4, the Weierstrass surface state in the whole BZ with the illustrated bulk double-Weyl points at the pole and zero. The isofrequency surface loops have alternating orientations as the frequency changes. Two loops are plotted in green that match the calculation results in Figs. 3(b) and 3(c). This indicates that the surface phonons propagate towards different directions at different energies.

Conclusion.— We predicted topological phonons in both acoustic and optical branches of a family of existing crystalline materials: transition-metal monosilicides, that was previously studied as thermal-electric materials [57,58] and superconductors [59]. Experimentally, bulk phonons can be measured by neutron scattering [23] or x-ray scattering [60] and surface phonons can be probed by high resolution electron energy loss spectroscopy [24], helium scattering [61], or THz spectroscopy [62,63]. Low-temperature measurements might be helpful to minimize the anharmonic effects (see Supplemental Material [51]). Topological bulk phonons could be advantageous for phonon transport [64], around the frequencies of the Weyl nodes, due to their linear dispersions and reduced backscattering. Topological surface phonons can potentially enhance electron-phonon interactions at material

interfaces, since they are guaranteed to localize at the surface [65,66]. This is beneficial, for example, to interfacial superconductivity [67].

We thank Jiawei Zhou, Yuanfeng Xu, Gregory Moore, Shiyang Li, Xuetao Zhu for useful discussion. This work was supported National key R&D Program of China under Grants No. 2016YFA0302400 (C. F., L. L.), No. 2016YFA0300600 (C. F., H. W.), and No. 2017YFA0303800 (L. L.), NSFC under Grants No. 11674370 (C. F.), No. 11421092 (T. Z., H. W., Z. F.), and No. 11721404 (L. L.), the National 973 program of China No. 2013CB921700 (Z. F.), the Yale Postdoctoral Prize Fellowship (A. A.), and the National Thousand-Young Talents Program of China (C. F., L. L.).

Note added.—Recently, we became aware of two related works reporting multiple Weyl fermions, instead of phonons, in the same material system [68,69].

*cfang@iphy.ac.cn

†linglu@iphy.ac.cn

- [1] M. Z. Hasan and C. L. Kane, Colloquium: Topological insulators, *Rev. Mod. Phys.* **82**, 3045 (2010).
- [2] X.-L. Qi and S.-C. Zhang, Topological insulators and superconductors, *Rev. Mod. Phys.* **83**, 1057 (2011).
- [3] C.-K. Chiu, J. C. Y. Teo, A. P. Schnyder, and S. Ryu, Classification of topological quantum matter with symmetries, *Rev. Mod. Phys.* **88**, 035005 (2016).
- [4] A. Bansil, H. Lin, and T. Das, Colloquium: Topological band theory, *Rev. Mod. Phys.* **88**, 021004 (2016).
- [5] L. Lu, J. D. Joannopoulos, and M. Soljačić, Topological photonics, *Nat. Photonics* **8**, 821 (2014).
- [6] L. Lu, J. D. Joannopoulos, and M. Soljačić, Topological states in photonic systems, *Nat. Phys.* **12**, 626 (2016).
- [7] S. D. Huber, Topological mechanics, *Nat. Phys.* **12**, 621 (2016).
- [8] E. Prodan and C. Prodan, Topological Phonon Modes and Their Role in Dynamic Instability of Microtubules, *Phys. Rev. Lett.* **103**, 248101 (2009).
- [9] C. L. Kane and T. C. Lubensky, Topological boundary modes in isostatic lattices, *Nat. Phys.* **10**, 39 (2014).
- [10] B. G.-g. Chen, N. Upadhyaya, and V. Vitelli, Nonlinear conduction via solitons in a topological mechanical insulator, *Proc. Natl. Acad. Sci. U.S.A.* **111**, 13004 (2014).
- [11] Z. Yang, F. Gao, X. Shi, X. Lin, Z. Gao, Y. Chong, and B. Zhang, Topological Acoustics, *Phys. Rev. Lett.* **114**, 114301 (2015).
- [12] P. Wang, L. Lu, and K. Bertoldi, Topological Phononic Crystals with One-Way Elastic Edge Waves, *Phys. Rev. Lett.* **115**, 104302 (2015).
- [13] M. Xiao, W.-J. Chen, W.-Y. He, and C. T. Chan, Synthetic gauge flux and Weyl points in acoustic systems, *Nat. Phys.* **11**, 920 (2015).
- [14] L. M. Nash, D. Kleckner, A. Read, V. Vitelli, A. M. Turner, and W. T. M. Irvine, Topological mechanics of gyroscopic metamaterials, *Proc. Natl. Acad. Sci. U.S.A.* **112**, 14495 (2015).

- [15] R. Süsstrunk and S. D. Huber, Observation of phononic helical edge states in a mechanical topological insulator, *Science* **349**, 47 (2015).
- [16] S. H. Mousavi, A. B. Khanikaev, and Z. Wang, Topologically protected elastic waves in phononic metamaterials, *Nat. Commun.* **6**, 8682 (2015).
- [17] R. Fleury, A. B. Khanikaev, and A. Alù, Floquet topological insulators for sound, *Nat. Commun.* **7**, 11744 (2016).
- [18] D. Z. Rocklin, B. G.-g. Chen, M. Falk, V. Vitelli, and T. C. Lubensky, Mechanical Weyl Modes in Topological Maxwell Lattices, *Phys. Rev. Lett.* **116**, 135503 (2016).
- [19] C. He, X. Ni, H. Ge, X.-C. Sun, Y.-B. Chen, M.-H. Lu, X.-P. Liu, and Y.-F. Chen, Acoustic topological insulator and robust one-way sound transport, *Nat. Phys.* **12**, 1124 (2016).
- [20] J. Lu, C. Qiu, L. Ye, X. Fan, M. Ke, F. Zhang, and Z. Liu, Observation of topological valley transport of sound in sonic crystals, *Nat. Phys.* **13**, 369 (2016).
- [21] R. Süsstrunk and S. D. Huber, Classification of topological phonons in linear mechanical metamaterials, *Proc. Natl. Acad. Sci. U.S.A.* **113**, E4767 (2016).
- [22] P. Brüesch, *Phonons: Theory and Experiments II. Experiments and Interpretation of Experimental Results*, Springer Series in Solid-State Sciences vol. 65 (Springer, Berlin, 1986).
- [23] O. Delaire, I. I. Al-Qasir, A. F. May, C. W. Li, B. C. Sales, J. L. Niedziela, J. Ma, M. Matsuda, D. L. Abernathy, and T. Berlijn, Heavy-impurity resonance, hybridization, and phonon spectral functions in $\text{Fe}_{1-x}\text{M}_x\text{Si}$ ($M = \text{Ir}, \text{Os}$), *Phys. Rev. B* **91**, 094307 (2015).
- [24] X. Zhu, Y. Cao, S. Zhang, X. Jia, Q. Guo, F. Yang, L. Zhu, J. Zhang, E. W. Plummer, and J. Guo, High resolution electron energy loss spectroscopy with two-dimensional energy and momentum mapping, *Rev. Sci. Instrum.* **86**, 083902 (2015).
- [25] L. Zhang, J. Ren, J.-S. Wang, and B. Li, Topological Nature of the Phonon Hall Effect, *Phys. Rev. Lett.* **105**, 225901 (2010).
- [26] N. Li, J. Ren, L. Wang, G. Zhang, P. Hänggi, and B. Li, Colloquium: Phononics: Manipulating heat flow with electronic analogs and beyond, *Rev. Mod. Phys.* **84**, 1045 (2012).
- [27] Y. Liu, Y. Xu, S.-C. Zhang, and W. Duan, Model for topological phononics and phonon diode, *Phys. Rev. B* **96**, 064106 (2017).
- [28] W.-C. Ji and J.-R. Shi, Topological phonon modes in a two-dimensional wigner crystal, *Chin. Phys. Lett.* **34**, 036301 (2017).
- [29] S. Murakami, Phase transition between the quantum spin hall and insulator phases in 3d: Emergence of a topological gapless phase, *New J. Phys.* **9**, 356 (2007).
- [30] X. Wan, A. M. Turner, A. Vishwanath, and S. Y. Savrasov, Topological semimetal and Fermi-arc surface states in the electronic structure of pyrochlore iridates, *Phys. Rev. B* **83**, 205101 (2011).
- [31] S.-Y. Xu, I. Belopolski, N. Alidoust, M. Neupane, G. Bian, C. Zhang, R. Sankar, G. Chang, Z. Yuan, C.-C. Lee *et al.*, Discovery of a Weyl fermion semimetal and topological Fermi arcs, *Science* **349**, 613 (2015).
- [32] B. Q. Lv, H. M. Weng, B. B. Fu, X. P. Wang, H. Miao, J. Ma, P. Richard, X. C. Huang, L. X. Zhao, G. F. Chen *et al.*, Experimental Discovery of Weyl Semimetal TaAs, *Phys. Rev. X* **5**, 031013 (2015).
- [33] L. Lu, Z. Wang, D. Ye, L. Ran, L. Fu, J. D. Joannopoulos, and M. Soljačić, Experimental observation of weyl points, *Science* **349**, 622 (2015).
- [34] A. A. Soluyanov, D. Gresch, Z. Wang, Q. Wu, M. Troyer, X. Dai, and B. A. Bernevig, Type-ii weyl semimetals, *Nature (London)* **527**, 495 (2015).
- [35] A. A. Burkov, Topological semimetals, *Nat. Mater.* **15**, 1145 (2016).
- [36] K. Deng, G. Wan, P. Deng, K. Zhang, S. Ding, E. Wang, M. Yan, H. Huang, H. Zhang, Z. Xu, J. Denlinger, A. Fedorov, H. Yang, W. Duan, H. Yao, Y. Wu, S. Fan, H. Zhang, X. Chen, and S. Zhou, Experimental observation of topological fermi arcs in type-ii Weyl semimetal MoTe_2 , *Nat. Phys.* **12**, 1105 (2016).
- [37] B. Bradlyn, J. Cano, Z. Wang, M. G. Vergniory, C. Felser, R. J. Cava, and B. A. Bernevig, Beyond dirac and Weyl fermions: Unconventional quasiparticles in conventional crystals, *Science* **353**, aaf5037 (2016).
- [38] R. M. Geilhufe, S. S. Borysov, A. Bouhon, and A. V. Balatsky, Data mining for three-dimensional organic dirac materials: Focus on space group 19, *Sci. Rep.* **7**, 7298 (2017).
- [39] Z. K. Liu, B. Zhou, Y. Zhang, Z. J. Wang, H. M. Weng, D. Prabhakaran, S.-K. Mo, Z. X. Shen, Z. Fang, X. Dai *et al.*, Discovery of a three-dimensional topological dirac semimetal, Na_3Bi , *Science* **343**, 864 (2014).
- [40] G. Xu, H. Weng, Z. Wang, X. Dai, and Z. Fang, Chern Semimetal and the Quantized Anomalous Hall Effect in HgCr_2Se_4 , *Phys. Rev. Lett.* **107**, 186806 (2011).
- [41] C. Fang, M. J. Gilbert, X. Dai, and B. A. Bernevig, Multi-Weyl Topological Semimetals Stabilized by Point Group Symmetry, *Phys. Rev. Lett.* **108**, 266802 (2012).
- [42] W.-J. Chen, M. Xiao, and C. T. Chan, Experimental observation of robust surface states on photonic crystals possessing single and double Weyl points, *arXiv:1512.04681*.
- [43] S.-M. Huang, S.-Y. Xu, I. Belopolski, C.-C. Lee, G. Chang, T.-R. Chang, B. Wang, N. Alidoust, G. Bian, and M. Neupane *et al.*, New type of Weyl semimetal with quadratic double Weyl fermions, *Proc. Natl. Acad. Sci. U.S.A.* **113**, 1180 (2016).
- [44] L. Pauling and A. M. Soldate, The nature of the bonds in the iron silicide, FeSi , and related crystals, *Acta Crystallogr.* **1**, 212 (1948).
- [45] Y. N. Zhao, H. L. Han, Y. Yu, W. H. Xue, and T. Gao, First-principles studies of the electronic and dynamical properties of monosilicides MSi ($M = \text{Fe}, \text{Ru}, \text{Os}$), *Europhys. Lett.* **85**, 47005 (2009).
- [46] X. Gonze and C. Lee, Dynamical matrices, born effective charges, dielectric permittivity tensors, and interatomic force constants from density-functional perturbation theory, *Phys. Rev. B* **55**, 10355 (1997).
- [47] G. Kresse and J. Furthmüller, Efficient iterative schemes for *ab initio* total-energy calculations using a plane-wave basis set, *Phys. Rev. B* **54**, 11169 (1996).

- [48] A. A. Soluyanov and D. Vanderbilt, Computing topological invariants without inversion symmetry, *Phys. Rev. B* **83**, 235401 (2011).
- [49] R. Yu, X. L. Qi, A. Bernevig, Z. Fang, and X. Dai, Equivalent expression of \mathbb{Z}_2 topological invariant for band insulators using the non-Abelian Berry connection, *Phys. Rev. B* **84**, 075119 (2011).
- [50] W. Gao, M. Lawrence, B. Yang, F. Liu, F. Fang, B. Béri, J. Li, and S. Zhang, Topological Photonic Phase in Chiral Hyperbolic Metamaterials, *Phys. Rev. Lett.* **114**, 037402 (2015).
- [51] See Supplemental Material at <http://link.aps.org/supplemental/10.1103/PhysRevLett.120.016401> for more detailed discussions.
- [52] A. Togo and I. Tanaka, First principles phonon calculations in materials science, *Scr. Mater.* **108**, 1 (2015).
- [53] M. P. L. Sancho, J. M. Lopez Sancho, J. M. L. Sancho, and J. Rubio, Highly convergent schemes for the calculation of bulk and surface Green functions, *J. Phys. F* **15**, 851 (1985).
- [54] M. P. L. Sancho, J. M. Lopez Sancho, and J. Rubio, Quick iterative scheme for the calculation of transfer matrices: application to Mo (100), *J. Phys. F* **14**, 1205 (1984).
- [55] Q. Wu, S. Zhang, H.-F. Song, M. Troyer, and A. A. Soluyanov, WannierTools: An open-source software package for novel topological materials, [arXiv:1703.07789](https://arxiv.org/abs/1703.07789).
- [56] C. Fang, L. Lu, J. Liu, and L. Fu, Topological semimetals with helicoid surface states, *Nat. Phys.* **12**, 936 (2016).
- [57] R. Wolfe, J. H. Wernick, and S. E. Haszko, Thermoelectric properties of FeSi, *Phys. Lett.* **19**, 449 (1965).
- [58] B. C. Sales, O. Delaire, M. A. McGuire, and A. F. May, Thermoelectric properties of Co-, Ir-, and Os-doped FeSi alloys: Evidence for strong electron-phonon coupling, *Phys. Rev. B* **83**, 125209 (2011).
- [59] P. A. Frigeri, D. F. Agterberg, A. Koga, and M. Sigrist, Superconductivity without Inversion Symmetry: MnSi versus CePt₃Si, *Phys. Rev. Lett.* **92**, 097001 (2004).
- [60] M. Mohr, J. Maultzsch, E. Dobardžić, S. Reich, I. Milošević, M. Damnjanović, A. Bosak, M. Krisch, and C. Thomsen, Phonon dispersion of graphite by inelastic x-ray scattering, *Phys. Rev. B* **76**, 035439 (2007).
- [61] U. Harten and J. P. Toennies, Surface phonons on GaAs (110) measured by inelastic helium atom scattering, *Europhys. Lett.* **4**, 833 (1987).
- [62] L. Wu, M. Salehi, N. Koirala, J. Moon, S. Oh, and N. P. Armitage, Quantized Faraday and Kerr rotation and axion electrodynamics of a 3D topological insulator, *Science* **354**, 1124 (2016).
- [63] L. Wu, W.-K. Tse, M. Brahlek, C. M. Morris, R. V. Aguilar, N. Koirala, S. Oh, and N. P. Armitage, High-Resolution Faraday Rotation and Electron-Phonon Coupling in Surface States of the Bulk-Insulating Topological Insulator Cu_{0.02}Bi₂Se₃, *Phys. Rev. Lett.* **115**, 217602 (2015).
- [64] A. Chaudhuri, A. Kundu, D. Roy, A. Dhar, J. L. Lebowitz, and H. Spohn, Heat transport and phonon localization in mass-disordered harmonic crystals, *Phys. Rev. B* **81**, 064301 (2010).
- [65] W. Kress, F. W. de Wette, W. Kress, and F. W. de Wette, *Surface Phonons*, Springer Series in Surface Sciences 21, 1st ed. (Springer-Verlag, Heidelberg, Berlin 1991).
- [66] G. Resta, S.-T. Pi, X. Wan, and S. Y. Savrasov, High surface conductivity of Fermi arc electrons in Weyl semimetals, [arXiv:1708.02415](https://arxiv.org/abs/1708.02415).
- [67] S. Zhang, J. Guan, X. Jia, B. Liu, W. Wang, F. Li, L. Wang, X. Ma, Q. Xue, J. Zhang *et al.*, Role of SrTiO₃ phonon penetrating into thin FeSe films in the enhancement of superconductivity, *Phys. Rev. B* **94**, 081116 (2016).
- [68] G. Chang, S.-Y. Xu, B. J. Wieder, D. S. Sanchez, S.-M. Huang, I. Belopolski, T.-R. Chang, S. Zhang, A. Bansil, H. Lin, and M. Z. Hasan, Unconventional Chiral Fermions and Large Topological Fermi Arcs in RhSi, *Phys. Rev. Lett.* **119**, 206401 (2017).
- [69] P. Tang, Q. Zhou, and S.-C. Zhang, Multiple Types of Topological Fermions in Transition Metal Silicides, *Phys. Rev. Lett.* **119**, 206402 (2017).